XeF_2 etching of Si(111): The geometric structure of the reaction layer

C. W. Lo, D. K. Shuh,* V. Chakarian, T. D. Durbin, P. R. Varekamp, and J. A. Yarmoff
Department of Physics, University of California, Riverside, California 92521
and Materials Sciences Division, Lawrence Berkeley Laboratory, Berkeley, California 94720
(Received 22 September 1992; revised manuscript received 6 January 1993)

Si(111)-7×7 is exposed to XeF_2 in ultrahigh vacuum and examined with soft-x-ray photoelectron spectroscopy (SXPS) and photon-stimulated desorption (PSD). The exposures encompass the entire range from chemisorption to steady-state etching. By taking into account the different surface sensitivities of SXPS and PSD, the microscopic structure of the surface fluorosilyl reaction layer is obtained as a function of exposure, and the reaction process is modeled. It is found that the reaction-layer structure passes through four distinct exposure regimes. Steric hindrance between the F atoms of neighboring fluorosilyl groups and defects in the substrate are responsible for the evolution of the reaction-layer structure. When steady-state etching is reached, the reaction layer evolves to a "tree" structure of fluorosilyl chains terminated at the surface by SiF_3 groups.

I. INTRODUCTION

An understanding of the basic physics and chemistry of the surface reactions involved in the dry etching of semiconductors is needed in order to produce smaller and faster microelectronic devices. To selectively etch silicon in a plasma reactor, fluorine-containing gases, such as CF_4 or NF_3, are employed. Because of the simultaneous presence of ions, radicals, molecules, and an electromagnetic field, the etching mechanism is fairly complex. The primary chemical reaction, however, is between Si and atomic fluorine (F).

Numerous studies have focused on the spontaneous etching of Si by atomic F.[1] In particular, experiments conducted in ultrahigh vacuum (UHV) have the advantage of eliminating any complications resulting from the presence of background gases. In many UHV studies, XeF_2 has been employed as a source of high-purity atomic F.[2–7] Although the Si etching rates for XeF_2 and atomic F are different,[8] the surface chemical mechanisms are similar, as they both spontaneously etch Si at room temperature and have similar reaction products.[1] XeF_2, however, is considerably easier to employ in UHV than is atomic F. A microwave discharge is required to produce atomic F,[9] while XeF_2 can be introduced through a leak valve, since it is a solid with a room-temperature vapor pressure of a few Torr.

The gas-phase products produced in the spontaneous etching of Si by XeF_2 at room temperature are primarily SiF_4 (~85%), but also include Si_2F_6, Si_3F_8, and radicals.[4,7,9] The etching process proceeds through the formation of a surface reaction layer consisting of the fluorosilyl intermediate species SiF, SiF_2, and SiF_3.[6] Although the steady-state reaction layer thickness was roughly estimated at ~7 monolayers (ML) in Ref. 6, the actual thickness and structure of the layer was not determined. The growth of the fluorosilyl layer is aided by the formation of substrate defects via the heat liberated by the exothermic Si-F surface reaction.[10,11]

Earlier studies of the surface reaction layer have focused either solely on the initial reaction of XeF_2 with Si (Refs. 12 and 13) or on the steady-state etching regime.[5,6] In the present work, the evolution of the geometric structure of the fluorosilyl reaction layer is investigated over the entire range of XeF_2 exposures with both soft-x-ray photoemission spectroscopy (SXPS) and photon-stimulated desorption (PSD). Since SXPS and PSD each have different surface sensitivities, by comparing the results, a depth profile of the reaction layer composition is obtained. After taking this structure into account, a semiquantitative determination of the coverage of each SiF_x species is achieved through a careful analysis of Si $2p$ core-level SXPS spectra. It is found that, as the reaction proceeds from the initial chemisorption of F on Si(111)-7×7 to steady-state etching, the reaction layer passes through four distinct structural regimes and the substrate evolves from crystalline to disordered. A model of the reaction process, based on the evolution of the reaction layer and substrate structures, is developed.

II. EXPERIMENTAL PROCEDURE

The experimental data were collected on beamline UV-8b at the National Synchrotron Light Source at Brookhaven National Laboratory in Upton, NY.[14] Monochromatic photons were selected by a 6-m toroidal grating monochromator. The endstation consists of a spectrometer chamber (base pressure 1×10^{-10} Torr), a preparation chamber (base pressure 5×10^{-10} Torr), and a dosing chamber (base pressure 1×10^{-9} Torr) that are connected by a UHV sample transfer system. The spectrometer chamber is equipped with an ellipsoidal mirror analyzer (EMA).[15]

SXPS and PSD were both collected with the EMA operating in an angle-integrating mode, in which particles are collected within a total angular acceptance cone

of 85°. SXPS spectra of the Si $2p$ core level were collected as energy distribution curves (EDC's) at a combined monochromator and analyzer energy resolution of better than 0.2 eV. A photon energy of 130 eV was used in order to optimize the surface sensitivity. This photon energy produces Si $2p$ photoelectrons with a kinetic energy approximately 30 eV above the Fermi level, which corresponds to the minimum escape depth.[16] For PSD measurements, the photon energy was scanned through the Si $2p$ absorption edge while all of the positively charged ions desorbed from the sample were collected. As previously determined by mass-spectroscopic measurements, F^+ is the only positively charged ion that desorbs from fluorinated Si as a consequence of electronic excitation.[17–19] In order to detect the positively charged ions, the electrical polarities of the analyzer were reversed, as described previously.[12] To ensure that F^+ ions emitted over all angles were collected, a -75-V bias was applied to the first grid of the analyzer. An additional -1000 V was applied to the front of the microchannel plate array in order to accelerate the ions into the detector, as well as to prevent background electrons from being collected.

The reaction of XeF_2 with Si is very sensitive to the presence of metallic impurities.[20] One source of metal contamination is chemical vapor transport of volatile metal fluorides formed by reaction of XeF_2 with the chamber walls, manipulators, sample holders, ion gauges, etc. To reduce these effects, the dosing chamber was passivated prior to the experiments by 1×10^{-4} Torr of XeF_2 for 30 min followed by exposure of a dispensable Si sample to 1×10^{-5} Torr of XeF_2 for 4 h. In addition, the pressure in the dosing chamber was measured with a cold cathode ion gauge in order to prevent tungsten contamination via WF_6, which is produced by reaction of XeF_2 with the hot filament of a conventional ion gauge. The pressure measurements using the cold cathode gauge were within an order of magnitude of the conventional ion gauge readings.

Si(111) wafers (n-type, P-doped, 1.0–1.3 Ω cm), cut within 0.25° of the low index plane were cleaned by degasing at 450 °C followed by Ohmic heating to 1050 °C to remove the native oxide and form the 7×7 reconstruction. Si $2p$ core level and valence-band SXPS spectra were used to verify the cleanness and crystallinity of the samples. The appearance of unique and well-resolved surface core-level shifts (SCLS's) in the $2p$ spectra indicates the formation of clean and well-ordered Si(111)-7×7.[21] Valence-band spectra were used to verify the absence of contaminants, such as carbon, oxygen, or metals. The sample was exposed to XeF_2 in the dosing chamber and transferred under UHV to the spectrometer chamber to collect the SXPS and PSD spectra. In order to monitor the development of the reaction layer, a single sample was exposed to increasing amounts of XeF_2 without cleaning between exposures. The exposures are reported in langmuirs (1 L = 1×10^{-6} Torr sec). The reproducibility was checked by repeating the experiment with a new sample. The samples initially had mirrorlike surfaces, but after receiving very large XeF_2 exposures, the surfaces resembled fine sandpaper when viewed under a microscope in air at a 20× magnification.

III. RESULTS

A. SXPS

In order to monitor the evolution of the reaction layer composition with XeF_2 exposure, the entire set of Si $2p$ core-level SXPS spectra were numerically fit to a sum of Gaussian-broadened Lorentzian spin-orbit split line shapes via a least-squares procedure. Each individual Si $2p$ spectrum is composed of a substrate component and a number of chemically shifted components that correspond to each of the chemically distinct states of Si present in the surface and near-surface regions of the sample. Each distinct $2p$ component is composed of both $2p_{1/2}$ and $2p_{3/2}$ levels as a result of the spin-orbit interaction. The separation and branching ratio between these levels are 0.61 and 0.52 eV, respectively, and are fixed throughout the fitting procedure.[21] Because of final-state effects, the apparent branching ratio is slightly different than the statistically expected ratio of 0.50.

Before fitting a Si $2p$ SXPS spectrum, the secondary-electron background is removed in a two-step process. In the first step, a measured background, which reveals the general shape of the secondary-electron distribution without including the secondary electrons generated by the $2p$ photoelectrons themselves, is subtracted from the raw data. Measured background spectra are collected over the same kinetic-energy range as the Si $2p$ spectra, but with a 10-eV lower photon energy, i.e., 120 eV, in order to avoid detection of the $2p$ photoelectrons. The second step in background subtraction is to numerically remove the secondary electrons generated by the Si $2p$ photoelectrons. This contribution to the background is simulated by fitting the background underneath the peaks to the integral of the peaks, and the region outside of the peaks to a polynomial plus a step function that is proportional to the total integrated area. The implicit assumption in this method is that the secondary-electron distribution underneath the peak is directly proportional to the integral of the peak, i.e., that the loss function is a constant.[22]

An inelastic loss feature, modeled by a Poisson distribution of fixed energy losses, is included on each of the Si $2p$ components for all spectra collected after XeF_2 exposures in excess of 90 L.[10] The inelastic loss feature results from the presence of trivalent Si defects at the reaction-layer–substrate interface and in the near-surface region of the substrate. The formation of these defects is discussed in detail in Ref. 10. The Poisson distribution is characterized by two parameters: (1) the energy loss per interaction $E_{\rm loss}$ and (2) the average number of interactions $N_{\rm int}$, which provides a rough measure of the concentration of defects. For all exposures below 700 000 L, a value of $E_{\rm loss}=0.30$ eV produces the best fits. Trivalent Si centers induce states in the gap at ~0.3 eV above the valence-band maximum (VBM) and at ~0.3 eV below the conduction-band minimum (CBM),[23,24] so that a photoelectron can lose energy by exciting an electron either from the VBM to a gap state or from a gap state to the CBM. A slightly different value for $E_{\rm loss}$ (0.35 eV) is found after the 700 000-L exposure. This may be related

to the presence of metallic contaminants deposited on the surface as a result of vapor-phase transport of metal fluorides. The presence of metallic impurities becomes significant only after very large exposures, and their effects are discussed in detail elsewhere.[20]

The fitting procedure yields peak positions, peak areas, both the Gaussian and Lorentzian contributions to the peak widths, and the value of N_{int}. Figures 1 and 2 show SXPS spectra collected from Si(111)-7×7 before and after XeF_2 exposure. The raw data, after background subtraction, are shown as dots, while each of the individual 2p components and the sum of the components are shown as solid lines. The dashed lines in Fig. 2 show the bulk component and its associated inelastic loss separately. The binding energies are given with respect to the bulk Si 2p level, so that they are independent of changes in electron kinetic energy induced by band bending. In the spectrum collected from the clean surface, shown in Fig. 1(a), there are two SCLS components S_1 and S_2 at binding energies of 0.35 and −0.69 eV. These SCLS's result from Si atoms located at particular sites of the 7×7 structure.[16,25] After exposure to XeF_2, up to four chemically shifted peaks, representing SiF, SiF_2, SiF_3, and SiF_4,

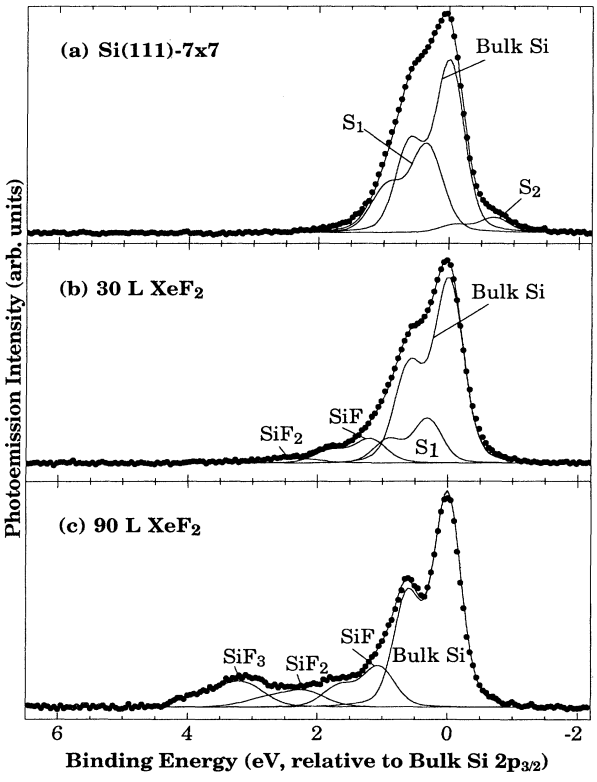

FIG. 1. Si 2p SXPS spectra collected from (a) clean Si(111)-7×7, (b) after a 30-L XeF_2 exposure at room temperature, and (c) after a 90-L exposure. The raw data, after background subtraction, are shown as filled circles, while the individual and sum of the components of a numerical fit to the data are shown as lines.

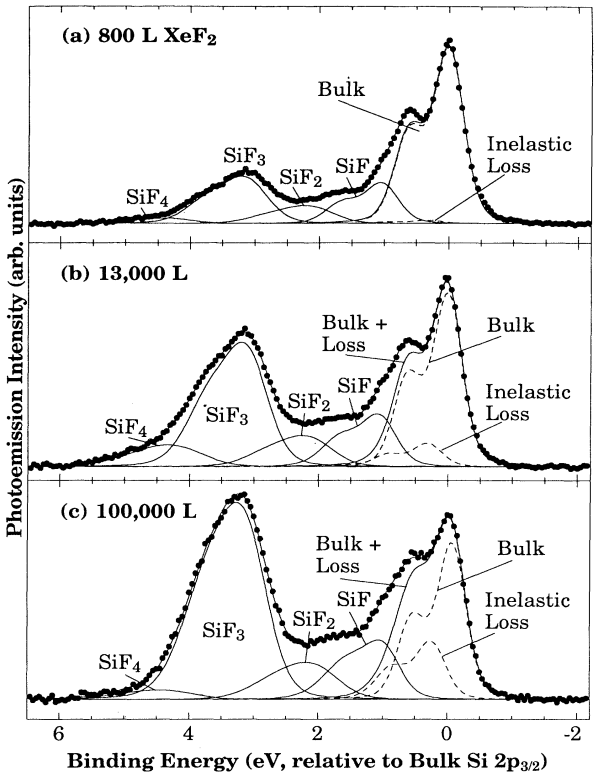

FIG. 2. Si 2p SXPS spectra collected from Si(111) after exposure to (a) 800 L, (b) 13 000 L, and (c) 100 000 L of XeF_2. The raw data, after background subtraction, are shown as filled circles, while the individual and sum of the components of a numerical fit to the data are shown as lines.

are observed, as the Si 2p core level is shifted by ~1 eV for each bond to F.[13] The binding-energy shifts determined for SiF, SiF_2, and SiF_3 after each exposure were consistent within ±0.10 eV, and are therefore independent of F coverage. The values obtained are 1.04, 2.11, and 3.12 eV, respectively. The shift found for the SiF_4 component was approximately 4.3 eV, and varied slightly with exposure.[20]

Spectra were collected from one sample after 30- and 90-L exposures and from a second sample after 100–700 000-L exposures. As shown in Fig. 1(b), after a 30-L exposure, S_2 disappears, S_1 is reduced and its binding energy is shifted to 0.32 eV, and SiF plus a small amount of SiF_2 appears. After a 90-L exposure, as shown in Fig. 1(c), the SCLS features are completely gone, while SiF, SiF_2, and SiF_3 are each present. Representative spectra collected after larger XeF_2 exposures are shown in Fig. 2. In these spectra, the concentrations of the higher fluorides increase, some SiF_4 is observed, and the intensity of the inelastic loss component becomes significant.

In Fig. 3, the evolution of the area of each SiF_x Si 2p component is shown as a function of the logarithm of the exposure. The data are normalized by dividing by the bulk Si 2p component, rather than shown on an absolute

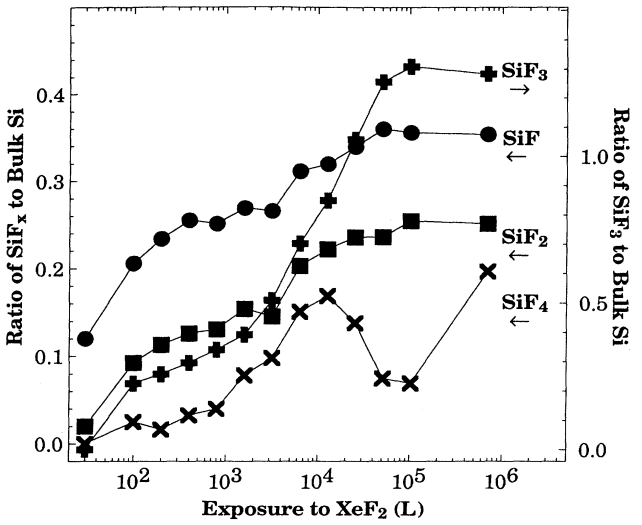

FIG. 3. The intensities of each of the SiF_x components of the Si $2p$ SXPS spectra, divided by the bulk Si $2p$ signal, shown as a function of exposure to XeF_2.

scale, in order to account for differences in sample repositioning, beam drift, etc. The SiF, SiF_2, and SiF_3 Si $2p$ areas each increase monotonically with exposure, while the SiF_4 area has a more complex behavior. The SiF and SiF_2 components roughly follow each other, while SiF_3 has a steeper slope in the 2000–100 000-L range.

In Fig. 4, the average number of inelastic losses experienced by the bulk Si $2p$ photoelectrons N_{int} is shown as a function of exposure. There are no significant inelastic losses observed until the exposure reaches ~2000 L, at which point N_{int} rises until about 100 000 L, where it stabilizes at ~0.32.

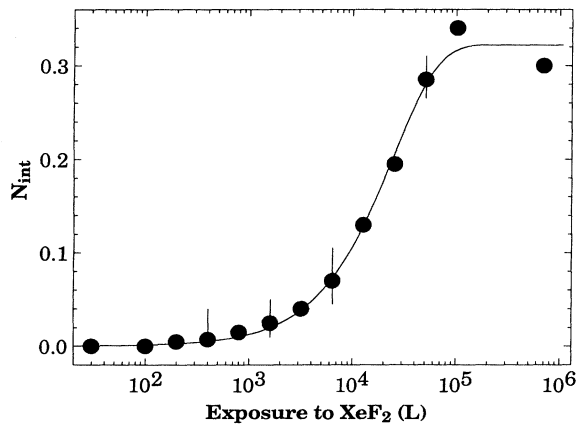

FIG. 4. The average number of interactions N_{int} in a Poisson distribution of inelastic losses, shown as a function of XeF_2 exposure. Representative error bars are shown by vertical lines. The solid line is a smooth curve drawn through the data points.

B. PSD

F^+ PSD spectra at the Si $2p$ edge produce the equivalent of localized near-edge x-ray absorption fine-structure spectra of the bonding Si atoms on the outermost surface, with very little contribution from subsurface atoms.[12,26] PSD spectra are collected by scanning the photon energy through the Si $2p$ absorption edge while measuring the total yield of F^+ ions desorbed from the surface. Si $2p$ excitations in SiF_x species decay via a localized interatomic Auger process[27] that induces the desorption of F^+ ions.[26] Because of the short mean free path of F^+, the ions that are detected result only from Si-F bond breaking in the extreme near-surface region so that only the outermost SiF_x groups contribute to the PSD spectra. The short mean free path is due to a combination of both neutralization of F^+ ions and reaction.

PSD spectra collected at the Si $2p$ edge contain absorption edge features that correspond to transitions from the $2p$ levels of the bonding Si atoms to either the CBM or to an unoccupied SiF_x molecular orbital. As an example, SXPS and PSD spectra collected after a 1600-L XeF_2 exposure are shown in Fig. 5. To illustrate the transitions to the CBM, the binding energy for the SXPS spectrum is given with respect to the CBM. The thresholds for absorption from Si $2p_{3/2}$ initial states to the CBM are indicated by (a)–(d) in the figure.[12,26] There are absorption edges corresponding to transitions from the $2p_{1/2}$ initial states, at 0.61 eV higher photon energy, but these are less distinct than the $2p_{3/2}$-initiated features, and are not indicated in order to minimize the clutter in the figure. In addition, there are transitions in the PSD spectra from

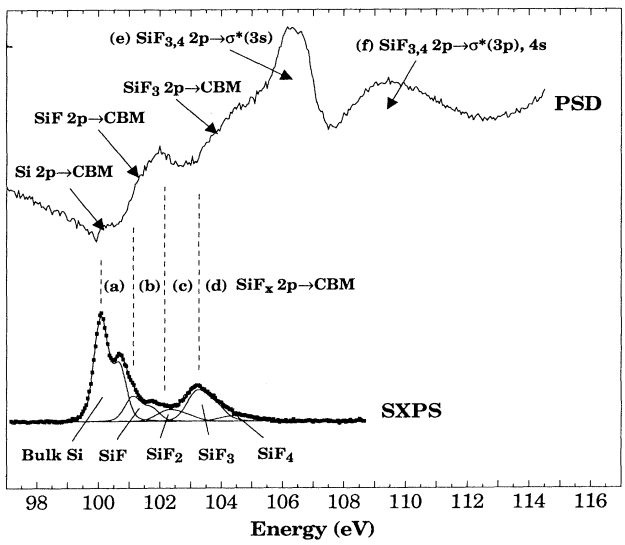

FIG. 5. PSD and SXPS spectra collected from Si(111) after a 1600-L XeF_2 exposure. In the PSD spectrum, there are six absorption edges (a)–(f) which correspond to different electronic transitions. In order to illustrate transitions to the CBM in the PSD spectra, the binding-energy scale in the SXPS spectrum is given with respect to the CBM.

(*e*) the Si 2*p* levels in SiF_3 and SiF_4 to the 3*s*-like σ^* state, and (*f*) the 2*p* levels in SiF_3 and SiF_4 to the 3*p*-like σ^* state.[12,26] The electronic structure of the quasimolecular SiF_3 adsorbate is sufficiently localized such that the σ^* molecular-orbital states, which exist in both gas-phase and condensed SiF_4,[28,29] are formed.

The intensities of the absorption edges in the PSD spectra are roughly proportional to the concentrations of SiF_x at the outermost surface. An exception is feature (*a*), which results from photon absorption in the Si substrate, producing secondary electrons that, in turn, induce ESD of F^+.[30] In the following analysis, absorption edges (*b*), (*c*), and (*d*) are used as a rough measure of the surface concentrations of SiF, SiF_2, and SiF_3, respectively. Since features (*e*) and (*f*) result from absorption by both surface SiF_3 and SiF_4, it is not straightforward to determine the relative concentrations of each of these species. However, by examining the shape of a PSD spectrum in the region of features (*e*) and (*f*), the presence of SiF_4 at the reaction layer surface can be ascertained. In particular, if there is a trace amount of SiF_4, as is the case for the data shown in Fig. 5, then feature (*e*) is larger than feature (*d*).

The entire set of PSD spectra, which were collected along with the corresponding SXPS spectra, is shown in Fig. 6. As the exposure increases, features (*b*) and (*c*) become less pronounced while feature (*d*) becomes more pronounced. After reaching steady-state etching, desorption is no longer visible at features (*b*) and (*c*). This indicates that the concentrations of SiF and SiF_2 at the very surface decrease and eventually vanish with increasing exposure, while the concentration of SiF_3 continuously increases until steady state is reached.

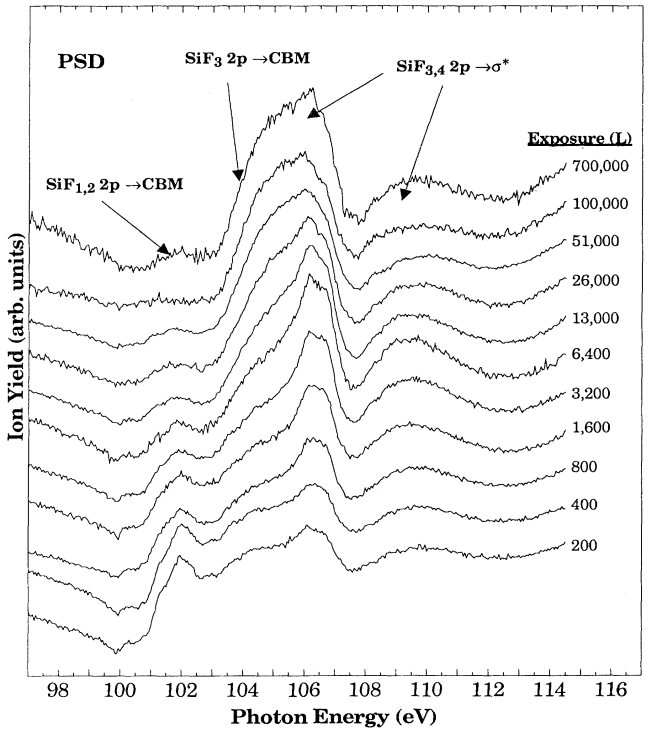

FIG. 6. PSD, as a function of XeF_2 exposure, collected from the same sample as the SXPS spectra shown in Fig. 3.

The SiF_4 signal in the PSD spectra initially increases to a maximum at ~6400 L and then decreases, i.e., it roughly follows the SXPS results. Since SiF_4 is a saturated molecule, it cannot be chemisorbed directly on the surface. The presence of SiF_4 features in the SXPS spectra would suggest that the molecules are somehow "trapped" in the reaction layer matrix.[6] The observation of SiF_4 in the PSD spectra, however, and the correspondence between the SXPS and PSD results for SiF_4 suggest that the molecules reside on top of the Si substrate. After the largest exposures, SiF_4 is seen on the surface because of the presence of metallic impurities, which can lead to the formation of $M^+(SiF_5)^-$ complexes.[20] The $(SiF_5)^-$ anion has a similar binding energy to SiF_4.[31] Although the maximum in the SiF_4 concentration at ~6400 L may also be due, in part, to metal impurities, there was no evidence of metallic impurities in the SXPS spectra, and if metal impurities were, in fact, the dominant cause of the SiF_4 signal in the PSD spectra, then a monotonic increase with exposure is expected. In addition, the behavior of the SiF_4 concentration is reproducible, which shows that it is unlikely to be completely due to impurities. It is probable, therefore, that there is either a trapping mechanism which occurs in conjunction with the particular geometric structure that exists after a ~6400-L exposure, or that a different type of pentavalent Si compound is formed. These effects are discussed in detail elsewhere.[20]

IV. DISCUSSION

A. Geometric structure of the reaction layer

Because of the difference in the relative surface sensitivities of the SXPS and PSD techniques, a comparison of the results indicates that the reaction layer structure is inhomogeneous. After low exposures (<2000 L), the reaction layer consists of a submonolayer amount of SiF_x groups, and SXPS and PSD results show similar ratios of the fluorosilyl species. As the reaction layer grows thicker, however, the areas of all of the Si 2*p* SiF_x components in the SXPS spectra increase monotonically, while the SiF and SiF_2 features in the PSD spectra decrease. After a 100 000-L exposure, the SiF and SiF_2 features in the PSD spectra are completely attenuated, while the SiF and SiF_2 SXPS components have reached their maximum intensity. The PSD results deviate from the SXPS results because the reaction layer develops a structure in which SiF and SiF_2 groups are located below SiF_3 groups.

The likely geometric configuration of the reaction layer at steady state is a "treelike" structure of fluorosilyl chains that are terminated by SiF_3 groups, as depicted in Fig. 7(a). Since SiF_3 is a chain terminator, assuming tetrahedral bonding, it is the most plausible species to be at the surface. There are a number of possible types of fluorosilyl chains, for example, —SiF_3, —SiF_2—SiF_3, =SiF—SiF_3, or =SiF—SiF_2—SiF_3. Some of these chains may be interconnected, as indicated in Fig. 7(a). Similar fluorosilyl chains have been observed in

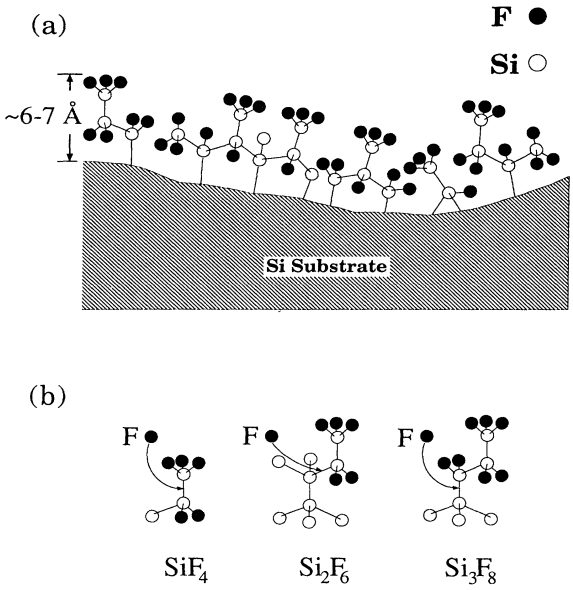

FIG. 7. (a) Schematic diagram of the "tree" structure, which consists of fluorosilyl chains terminated by SiF_3, residing on the macroscopically rough surface created by heavy etching. (b) Reaction processes that produce the gas-phase etching products SiF_4, Si_2F_6, and Si_3F_8 are shown schematically. Si atoms are represented by open circles and F atoms by filled circles.

molecular-dynamics simulations of the initial adsorption of 3.0-eV F incident on Si(100).[32]

The fact that SiF_4, Si_2F_6, and Si_3F_8 are each experimentally observed gas-phase reaction products lends further support for the "tree" structure. The major gas-phase etching product SiF_4 is produced when a F atom breaks the Si-Si bond that attaches an SiF_3 group to the surface. This is the most abundant reaction product, since each of the chains is terminated by SiF_3. The reaction products Si_2F_6 and Si_3F_8 are produced when the Si-Si bonds which attach —SiF_2—SiF_3 and —SiF_2—SiF_2—SiF_3 chains to the surface, respectively, are broken. These reaction steps are depicted in Fig. 7(b).

B. Semiquantitative analysis

A semiquantitative analysis of the layer thickness and the coverages of each of the fluorosilyl groups is obtained from the SXPS results. The areas of the Si 2*p* SXPS components shown in Fig. 3 are not directly proportional to the coverages of fluorosilyl groups in the reaction layer. Corrections need to be applied due to (1) differing Si 2*p* photoemission cross sections for each SiF_x component and (2) electron escape depth effects that occur with an inhomogeneous reaction layer. The semiquantitative analysis is obtained by using cross-section enhancements from the literature and electron escape depth effects based on the idea that the reaction layer evolves to a tree structure at steady state. From the results of this analysis, the likely distribution of the fluorosilyl chains in the reaction layer is determined.

The photoemission cross sections of the Si 2*p* level increase with oxidation state.[16] This cross-section enhancement has been observed for both Si_xO_y (Ref. 33) and SiF_x.[34] The measured enhancements for Si_xO_y and SiF_x at a photon energy of 130 eV, obtained from Refs. 33 and 34, respectively, are shown as a function of the Si 2*p* binding energy shift in Fig. 8. The cross-section enhancements were obtained by measuring photoelectron intensities of a submonolayer of fluorides (or oxides) as a function of photon energy, and then assuming that there is negligible enhancement at very high energies. Although data for SiF_4 were not presented in Ref. 34, its cross-section enhancement roughly estimated from the trend shown in Fig. 8, which is sufficient for the present analysis. The cross-section enhancements employed, relative to the bulk Si 2*p*, are 1.0, 1.3, 2.3, and 2.3 for SiF, SiF_2, SiF_3, and SiF_4, respectively.

After applying the cross-section corrections, the combined effects of the finite electron escape depth and the inhomogeneous reaction layer structure need to be accounted for. This correction is applied in different ways, depending on the reaction layer structure at a particular exposure level.

For estimating the coverage of a submonolayer of SiF_x groups on top of a Si substrate, the inhomogeneity of the reaction layer does not need to be explicitly considered. For exposures below 2000 L, there are less than 1 ML of total SiF_x groups adsorbed on the surface. Therefore, the ratio of the SiF_x Si 2*p* signal to the total Si 2*p* is used to calibrate the SiF_x coverages. As suggested by Himpsel *et al.*,[33] in order to determine submonolayer coverages, the area of a chemically shifted Si 2*p* component can be calibrated by the clean 7×7 surface SXPS spectrum, i.e., Fig. 2(a). The S_2 SCLS component in this spectrum corresponds to the seven rest atoms, or $\frac{7}{49}$ of a ML, in the 7×7 structure. As determined from the fitting procedure, this component has 0.050 of the total Si 2*p* intensity. Thus, 0.35 of the total Si 2*p* signal corresponds to 1

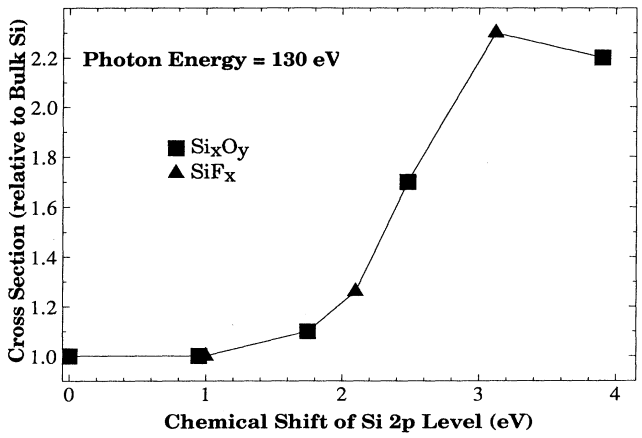

FIG. 8. Si 2*p* photoemission cross section (in arbitrary units) for $h\nu = 130$ eV shown as a function of the Si 2*p* chemical shift for oxygen and F bonding to Si. These data are from Refs. 33 and 34.

ML of adsorbed species, and the submonolayer coverages of SiF_x species are calibrated accordingly. Note that in this analysis, the attenuation of the Si 2*p* photoelectron signal by adsorbed F atoms is ignored since F attenuates the photoelectron signals from Si atoms in the SiF_x groups and the substrate nearly equally.

When the reaction layer thickness exceeds 1 ML, the inhomogeneity of the reaction layer needs to be considered. At steady state (> 30 000 L), we derive a simple calibration scheme based on a tree model of < 1 ML of SiF_3 species at the surface and 1 ML (total) of $SiF+SiF_2$ between the SiF_3 and the substrate Si. The SiF_3 coverage is therefore estimated by calculating the ratio of the SiF_3 Si 2*p* signal to the total Si 2*p* signal. Since SiF_3 equally attenuates the photoelectron signals from SiF, SiF_2, and the substrate, the coverages of SiF and SiF_2 are determined by ignoring the presence of SiF_3. Thus the ratio of SiF or SiF_2 Si 2*p* components to the sum of the SiF, SiF_2, and substrate components (rather than the total Si 2*p* intensity) is used to calculate their respective coverages, employing the calibration from above.

SiF_x coverages for exposures between 2000 and 30 000 L are more difficult to calibrate, however, because the reaction layer is intermediate between a monolayer SiF_x structure and the tree structure. In this intermediate regime, a portion of the SiF and SiF_2 groups are located on the outermost surface while the rest lie below SiF_3, and, moreover, the distributions of SiF and SiF_2 vary as a function of exposure. To overcome this problem, the SiF and SiF_2 coverages at 400 and 700 000 L are calibrated as described above. The coverages of SiF and SiF_2 in the intermediate regime are then linearly interpolated by assuming that they are directly proportional to their raw SXPS areas. The SiF_3 coverage, however, is calculated in the same manner as before, since SiF_3 is always located on the outermost surface.

Figure 9 shows the calibrated coverages of fluorosilyl groups in the reaction layer as a function of the logarithm of the XeF_2 exposure. These coverages, given in ML, refer to the number of fluorinated Si atoms and not to the total number of atoms. At steady state, the reaction layer is composed of approximately 0.65 ML of SiF, 0.37 ML of SiF_2, 0.73 ML of SiF_3, and 0.11 ML of SiF_4, which corresponds to a total of ~1.7 ML of SiF_x groups, or to a total F coverage of ~4.0 ML. As will be discussed below, the majority of the trees are either $=SiF—SiF_3$ or $=SiF—SiF_2—SiF_3$. By employing a simple model for the reaction-layer structure, such as is shown in Fig. 7, and by using Si-Si and Si-F bond distances,[35] which are fairly consistent from compound to compound, the reaction-layer thickness is estimated to be on the order of 6–7 Å. This estimate provides the thickness of the layer on a microscopic scale and does not take into account the total coverage of F that may be adsorbed on the high surface area of a macroscopically rough surface. Thus caution should be used in comparing these numbers to other results, as discussed below.

The uncertainties in the coverages given in Fig. 9 result from oversimplifying (1) the attenuation of the photoelectron signal due to adsorbed F and (2) the reaction-layer

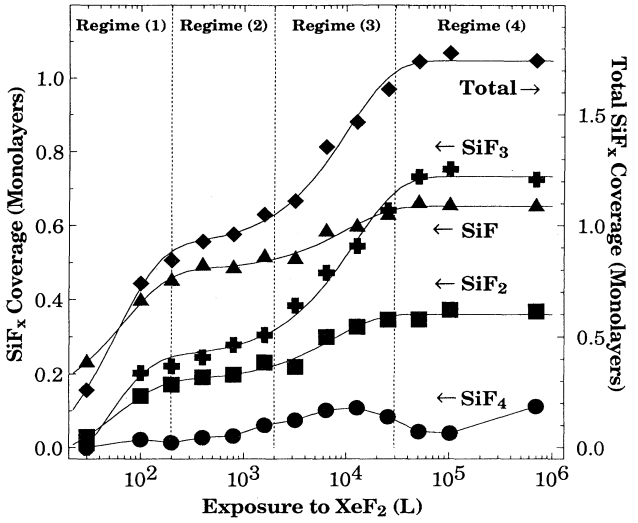

FIG. 9. The coverages of fluorosilyl groups in the reaction layer shown as a function of exposure. The coverages refer to ML's of SiF_x groups. The solid lines are smooth curves drawn through the data points.

structure at steady state. The SiF_3 coverage is estimated by calculating the ratio of the SiF_3 to the total Si 2*p* signal throughout. However, as the reaction layer develops a multilayer structure, the F bonded to SiF and SiF_2 attenuates all of the Si 2*p* components except SiF_3. Because of this, the SiF_3 coverage is slightly overestimated. Fortunately, this is only a minor effect, since the attenuation of the photoelectron signal due to F is far less than that due to Si, as known from the spectra collected from 1 ML of F adsorbed on Si. Second, in the above analysis, the SiF and SiF_2 coverages were assumed to total ~1 ML at steady state. There is, however, a small coverage of longer fluorosilyl chains, so that some of the SiF Si 2*p* signal is attenuated by SiF_2, etc., an effect that is not accounted for in the calibration. Nevertheless, if it were to be assumed that all of the SiF_2 species reside on top of SiF, the resultant SiF coverage would increase by only ~0.1 ML.

Winters and Coburn[1] and Engstrom, Nelson, and Engel,[36] using thermal desorption spectroscopy (TDS) and conventional x-ray photoelectron spectroscopy (XPS), also reported values for the thickness of the reaction layer. Their results, however, determined a reaction-layer thickness at steady state of about twice the F coverage than that found above, and larger values were determined with TDS than with XPS. This discrepancy is a consequence of different responses of the experimental techniques to the surface roughness that is created by large exposures. Of the three techniques employed to determine the adsorbed F coverage, TDS is the most sensitive to surface roughness, followed by XPS, and finally SXPS. In order to understand the discrepancies between the TDS, XPS, and SXPS results, the differences between these techniques are discussed.

In TDS, the total amount of adsorbed F is directly measured, while in both XPS and SXPS, the F coverage

is obtained from the ratio of a surface photoemission signal to a bulk signal. When the surface area increases due to roughening, the total coverage of adsorbed F, and thus the TDS signal, increases in proportion to the surface area. In both SXPS and XPS, on the other hand, surface roughness has less of an effect because surface photoemission signals are normalized to bulk signals, and both surface and bulk signals increase with increasing roughness, although not necessarily in proportion to the F coverage. In Refs. 1 and 36, the XPS and TDS intensities were calibrated to each other after a 50-L exposure, a point at which there is no surface roughening. Thus, in the presence of the roughening that exists after large XeF_2 exposures, TDS indicates a larger F coverage than does XPS.

XPS and SXPS also do not respond in the same way to roughness, since the relative surface sensitivities are considerably different. Photoelectrons originating from Si $2p$ have an escape depth of ≥ 13 Å in XPS,[37] and ~ 3 Å in SXPS.[16] The SXPS spectra were analyzed by comparing the shifted Si $2p$ components to the bulk $2p$ component. When the detected photoelectrons originate from the very surface of a roughened sample, as in SXPS, the large surface area acts to increase the contribution from both the reaction layer and the substrate nearly equally. In this manner, SXPS provides the thickness on a microscopic scale and is not sensitive to the presence of macroscopic roughness. On the other hand, the more bulk sensitive XPS technique behaves differently. The XPS data were analyzed by comparing the ratio of the total F $1s$ signal to the total Si $2p$.[1,36] When the surface area increases, the F $1s$ signal increases accordingly, but, providing that the roughness is on at least as small a scale as the XPS probe depth, the Si $2p$ intensity will not increase by a corresponding amount. Thus, higher F coverages are obtained from the more bulk sensitive XPS technique than from SXPS. Since the surface area of a roughened sample could easily be more than a factor of 2 enhanced over a flat surface, the observed discrepancies between SXPS and XPS can be accounted for by roughening.

A study of the etching of heavily doped Si with both TDS and XPS,[1] combined with a consideration of the different sensitivities of these techniques to surface roughness, suggests that etching of heavily doped p-type Si produces a particularly rough surface. In the work of Ref. 1, XPS indicates that the saturation coverage of F on heavily doped p-type samples is ~ 1.3 times higher than on n-type samples, in good agreement with the SXPS result of Ref. 5. On the other hand, when TDS was employed, three times as much F was found on p-type Si than on n-type Si. Since the differences between coverages determined by photoemission and TDS are a consequence of surface roughness, this comparison suggests that etching of heavily doped p-type Si produces a rougher surface than the etching of heavily doped n-type Si. Furthermore, the additional roughening on a heavily doped p-type surface must be on a larger scale than the XPS probe depth.

C. Reaction process

The XeF_2/Si etching reaction is divided into four exposure regimes, as depicted in Fig. 9: (1) the initial exposure regime (<200 L), during which F reacts with the 7×7 structure; (2) the quasiequilibrium regime, during which coverages of the surface fluorosilyl groups remain approximately constant (200–2000 L); (3) the transition to steady-state etching regime, during which the coverage of SiF_3 undergoes a large increase (2000–30 000 L); and (4) the steady-state etching regime ($>$ 30 000 L). The exposure scale in Fig. 9 is logarithmic, so that the transitions from one regime to the next actually occur more slowly at the higher exposure levels and the transitions themselves are not very sharp.

The reaction between F and Si is affected by the geometric and electronic structure of the surface region, and thus the species present on the surface do not simply reflect the bulk chemistry. The major reaction channel, which produces gaseous SiF_4, proceeds as a sequential addition of F.[38] These are basically reactions in which F withdraws electron density from Si. Thus, since the electron density at Si is reduced as each F bond is added, the rate of each reaction step is slower than the previous step.[7] This consideration of the chemical reactivities suggests that the conversion of SiF_3 to SiF_4 should be the rate limiting step, consistent with experimental observation,[6,39] and that at steady state, SiF_3 should be the most predominant species on the surface. However, the SiF_x coverages evolve in a complex manner, as shown in Fig. 9, because of the geometrical constraints of the surface. The details of these effects are discussed in the remainder of this paper.

The etching rate as a function of exposure also evolves in a complex manner as a consequence of electronic effects. Although the reaction layer is not fully formed until 30 000 L, etching actually begins after very low, on the order of 10 L, exposures.[4] In addition, it is observed that, after quickly reaching a maximum at ~ 40 L, the etching rate decreases with increasing exposure. From a simple consideration of the reaction-layer composition alone, it is expected that the production rate of SiF_4 would increase with exposure, since the coverage of the SiF_3 precursor species on the outermost surface increases. The decrease in the etching rate with exposure is largely the result of electronic effects, however, which are discussed separately.[40]

1. Initial exposure regime

At low exposures, the surface structure strongly influences the distribution of surface products, as was previously shown by comparing the low exposures of XeF_2 on various Si crystal faces.[13] In this section, the details of the manner in which the Si(111)-7×7 reconstruction is involved in the initial reaction are presented. By monitoring the SCLS components, observations are made of the initial F adsorption sites, the site-specific onset of etching, and the removal of the 7×7 structure.

The structure of the Si(111)-7×7 surface is best described by the dimer-adatom-stacking fault model.[41] In each unit cell, there are 12 adatoms and 7 rest atoms that have surface dangling bonds. The electronic properties of the rest atoms and adatoms have been investigated by scanning tunneling microscopy (STM) and valence-band

SXPS.[16,42] These investigations have shown that, because of electron donation from the dangling-bond orbital of the adatoms to the rest atoms, the adatoms are positively charged while the rest atoms are negatively charged. The partially filled adatom dangling bonds form a metallic surface state at the Fermi level.

The correlation between Si atoms at particular sites of the 7×7 structure and SCLS features in the SXPS spectra is not straightforward, however. Identifications of the S_1 and S_2 SCLS features have been made by both Himpsel *et al.*[16] and Karlsson *et al.*[25] Since rest atoms are negatively charged, their Si 2*p* binding energy is expected to be lower than that of bulk Si, so that, in both Refs. 16 and 25, S_2 is assigned to the rest atoms. Since the adatoms are positively charged, they are expected to have a higher binding energy than bulk Si. The area of S_1 is too large, however, to be accounted solely for by the adatoms. Himpsel *et al.* assigned S_1 to the adatoms plus photoelectrons originating from the bulk that experience energy loss by exciting electrons in the metallic surface state.[16] Karlsson *et al.* have suggested that, in addition, the S_1 structure includes a contribution from the 36 atoms in the second layer that are bonded to the adatoms.[25] These atoms are in a strained configuration, and can therefore have an altered Si 2*p* binding energy. Because they are in the second layer, however, their contribution to the Si 2*p* photoelectron signal is partially attenuated.

The changes in the SCLS intensities after the 30-L XeF_2 exposure are used to delineate the initial reaction of F with the 7×7 surface. As seen in Fig. 1(b), the S_1 SCLS area is reduced and S_2 is completely gone, while a small quantity of SiF and a negligible amount of SiF_2 are produced. The highly reactive dangling-bond sites are expected to be the first to adsorb F, which would form a surface covered by SiF. In order to form SiF_2, a Si-Si bond must be broken, which is a slow process that should not occur until after all of the dangling bonds have first been saturated. Since some SiF_2 is already present, a 30-L exposure has been more than sufficient to tie up the dangling bonds of all of the adatoms and rest atoms. The adatoms and rest atoms comprise $\frac{19}{49}$ of the 7×7 unit cell, or 0.39 ML, and the total measured SiF and SiF_2 coverages at this point are ~0.3 ML. Since these numbers are comparable, this result shows that the 7×7 structure is retained after the initial fluorination. If the 7×7 reconstruction had been removed, then a full ML of SiF would have been formed, as occurs when the cleaved Si(111)-2×1 surface is fluorinated.[13] A similar retention of the 7×7 structure has been seen in STM studies of Cl_2 chemisorption on Si(111)-7×7.[43] The S_1 SCLS is still present after the 30-L XeF_2 exposure, which is consistent with Karlsson's interpretation of the origin of S_1. Since all of the surface dangling bonds are tied up by F, neither metallic surface states nor adatoms can now contribute to S_1. The fact that a pronounced S_1 SCLS component remains is consistent with S_1 having a contributions from second layer atoms.

From 30 to 90 L, the primary reaction that occurs is between F and SiF species located at the adatom sites. These exposures represent the region of maximum etch rate[4] as well as the maximum rate of the buildup of the fluorosilyl layer, as seen by the slopes of the curves in Fig. 9. After a 90-L exposure, as seen in Fig. 1(c), S_1 completely disappears while SiF_2 and SiF_3 species become visible. The disappearance of S_1 indicates that the bonds between the adatoms and the second layer atoms have been severed. The high etch rate in this region is a consequence of the adatom structure. First, adatoms have three highly strained bonds to the second layer, which are relatively easy to break. Second, the adatoms protrude above the surface and have a greater lateral separation from each other than atoms in the underlying lattice, so that there is little barrier to overcome in order to adsorb F.

A microscopic picture of the F adsorption process, which explains the correlation between the creation of SiF_2 and SiF_3 species and the disappearance of S_1, is obtained from the data shown in Fig. 9. When the Si-Si bond between an SiF adatom group and the substrate is ruptured, two sites at which F can bond are created, at adatom and second layer Si atoms. These sites will quickly react with F and form SiF_2 on the outermost layer and SiF in the second layer. During this step, although one SiF and one SiF_2 group are created, one SiF group is removed, so that the total number of SiF species is unchanged. Further reaction of F with SiF_2 produces SiF_3 on the surface and another SiF in the second layer, so that during this step, one SiF and one SiF_3 group are created, while one SiF_2 group is removed. Thus the growth rates of SiF and SiF_3 should be equal as F reacts with the adatoms, which is confirmed by the fact that the slopes of the SiF and SiF_3 coverages in Fig. 9 are nearly equal in the initial exposure regime, a behavior that is not observed in any other exposure regime. Moreover, this picture shows why, because of the presence of adatoms on the 7×7 surface, higher SiF_2 and SiF_3 coverages are produced on this surface after small XeF_2 exposures than on the cleaved Si(111)-2×1 surface.[13]

2. *Quasiequilibrium exposure regime*

After the outermost atoms that comprise the 7×7 structure are removed, a quasiequilibrium between etching and the growth of the reaction layer, during which the coverages of the fluorosilyl groups remain relatively constant, is attained. In this regime, marked as (2) in Fig. 9, the reaction layer is ~1 ML thick, consists predominantly of SiF with only small amounts of SiF_2 and SiF_3, and the substrate is relatively crystalline. The amount of adsorbed F is limited because (1) F cannot react with Si atoms in a crystalline lattice and (2) there is steric hindrance between the F atoms of neighboring SiF_x groups on top of a crystalline substrate.

Theoretical studies by Van der Walle, McFeely, and Pantelides[44] and Schoolcraft and Garrison[45] both suggest that it is energetically unfavorable for F to break a Si-Si bond in a perfect crystal due to the geometrical constraints imposed by the surrounding Si network. Van der Walle, McFeely, and Pantelides indicate, however, that this geometric constraint is greatly reduced in a noncrys-

talline structure, for example, Si atoms at a surface or in a disordered substrate. Thus the transformation of the substrate lattice to a disordered structure has a great influence on the surface reaction, as will be seen in the transition regime (3).

The etching in the quasiequilibrium regime proceeds in an almost layer-by-layer fashion because F cannot react with Si atoms located below the surface. The substrate remains relatively crystalline, so that only those SiF_x groups located on the outermost surface are reactive. F reacts with these groups to form SiF_{x+1} on the surface and SiF in the second layer. Spontaneous etching occurs as the surface SiF_x groups become fully fluorinated to SiF_4.

Steric hindrance has a large influence on the reaction because the repulsion energy between the F atoms of neighboring SiF_x groups adsorbed on a crystalline substrate is quite high. As shown in a theoretical study by Wu and Carter,[46] these energies can be as high as 17 eV. Wu and Carter also showed, however, that the repulsion energy is greatly reduced if the SiF_x groups reside on a disordered substrate. Although the study in Ref. 46 was for Si(100), similar steric hindrance effects are expected for SiF_x groups on Si(111). The reason that SiF is the predominant surface species in the quasiequilibrium regime is that only a limited number of SiF_2 and/or SiF_3 groups can adsorb on a crystalline substrate because of steric hindrance. It is thus energetically unfavorable for the SiF_2 and SiF_3 coverages to increase past a certain point, despite the chemical impetus to do so. In addition, it is expected that the SiF_2 and SiF_3 groups will be separated from each other, with SiF groups in between, in order to further minimize steric hindrance.

3. *Transition to steady state*

In the transition regime, the number of trivalent Si defects in the near-surface region, which is indicated by N_{int}, greatly increases.[10] When the number of defects becomes sufficient, the quasiequilibrium is disrupted. Defects act to disorder the substrate in the near-surface region so that (1) F can be inserted below the surface in order to grow a thicker reaction layer and (2) steric hindrance between neighboring SiF_x groups is decreased, which enables the SiF_3 coverage to grow. Steric hindrance between SiF_3 groups is reduced further if the SiF_3 is located at the end of a long fluorosilyl chain, since such a structure is flexible. As a result, in the transition regime, the tree structure grows to replace the monolayer SiF_x structure and the reaction layer thickness increases to ~ 2 ML. As seen by comparing Figs. 4 and 9, the increase of the SiF_3 coverage correlates with the number of trivalent Si defects. While the defects allow the SiF_3 coverage to increase, the steric hindrance between SiF_3 groups induces the lattice stress needed to stabilize the defects.[10] When the SiF_3 coverage and the defect concentration attain equilibrium, steady-state etching is achieved.

There are two mechanisms through which trivalent Si defects are created in the near-surface region.[10] The first mechanism occurs as a F atom ruptures a Si-Si bond and attaches to one of the Si atoms leaving the other with a dangling bond. If the reaction layer is thin, this dangling bond will quickly be tied up by another incoming F atom. For a Si-Si bond broken near the bottom of a thick reaction layer, however, an appreciable concentration of dangling bonds can build up since the flux of F reaching the reaction-layer–substrate interface region is attenuated by the reaction layer. Trivalent Si defects formed by this mechanism are located either in the reaction layer or at the interface.

The second defect formation mechanism occurs as a consequence of the excess thermal energy liberated from the formation of exothermic Si-F bonds, and produces defects both at the interface and in the near-surface region of the substrate.[10,11] Energy dissipation through Si via phonon excitation is relatively slow (on the order of several hundred picoseconds),[47] so that the several electron volts of energy released by Si-F bond formation can be sufficiently localized to weaken or rupture another Si-Si bond.[11] Accompanying the breaking of a Si-Si bond, the surrounding Si lattice relaxes in order to reduce the stress built up by F adsorption. The trivalent Si defects created by the excess heat of reaction are thus stabilized as the surrounding lattice distorts. This mechanism is critical to the reaction process, since defects located below the interface are essential for the buildup of the fluorosilyl chains.

4. *Steady-state etching*

When the tree structure is completely developed, steady-state etching is achieved. Continuous etching produces a macroscopically disordered surface, as observed visually and illustrated in Fig. 7. As seen in Fig. 9, the reaction layer at steady state has an average thickness of ~ 2 ML of SiF_x species, and is composed of SiF, SiF_2, and SiF_3 in ratios of approximately 2:1:2. These ratios suggest that the tree structure consists primarily of a 1:1 mixture of $=SiF—SiF_3$ and $=SiF—SiF_2—SiF_3$ fluorosilyl chains. It is probable, however, that there are also $—SiF_3$, $—SiF_2—SiF_3$, $—SiF_2—SiF_2—SiF_3$, and various interconnected chains in the reaction layer.

Based on the tree structure and the assumption of sequential addition of F, the following cyclic reaction channel for producing the major gaseous product SiF_4 is proposed. As F breaks the Si-Si bond between an SiF_3 group and the underlying SiF_x species, it produces a volatile SiF_4 molecule and a dangling bond on the SiF_x group to which it was attached. This group will then quickly bond with another F atom and form SiF_{x+1}. This SiF_{x+1} group is most likely SiF_3, since the outer surface of the reaction layer is terminated almost exclusively by SiF_3. Thus a chain in which the second fluorosilyl species is SiF_2 is the primary precursor for the production of SiF_4. The most abundant chain of this type is $=SiF—SiF_2—SiF_3$. A cyclic etching process, in which the tree structure is maintained, is as follows:

$$\text{Substrate}=SiF—SiF_2—SiF_3+F \rightarrow \text{Substrate}=SiF—Si^*F_2+SiF_4(\text{gas}) , \quad (1)$$

$$\text{Substrate}{=}\text{SiF—Si}^{*}\text{F}_2+\text{F}\rightarrow\text{Substrate}{=}\text{SiF—SiF}_3\ , \tag{2}$$

$$\text{Substrate}{=}\text{SiF—SiF}_3+\text{F}\rightarrow\text{Substrate—SiF}_2\text{—SiF}_3\ , \tag{3}$$

$$\text{Substrate—SiF}_2\text{—SiF}_3+\text{F}\rightarrow\text{Substrate}{=}\text{SiF—SiF}_2\text{—SiF}_3\ , \tag{4}$$

where the asterisk represents the dangling bond created when SiF_4 evolves. Since this dangling bond is quickly tied up to form SiF_3, there is insufficient SiF_2 on the surface to be observed in PSD. It should be pointed out, however, that the above process is a simplified model for illustrating the primary reaction channel. In reality, since there are other types of fluorosilyl chains as well as interconnected chains, numerous reaction channels are involved.

To produce the minor gas-phase products Si_2F_6 and Si_3F_8 longer fluorosilyl chains are needed. The reaction layer structures involved, however, do not make a major contribution to the overall SiF_x coverages because the combined branching ratio of these two processes is less than 15%.[4,7,9] Moreover, the processes which produce Si_2F_6 and Si_3F_8 are not cyclic. If they were, the reaction layer would have a tree structure consisting of longer fluorosilyl chains than those observed.

V. SUMMARY

The geometric structure of the surface reaction layer as a function of XeF_2 exposure is investigated with SXPS and PSD. The development of the reaction layer is divided into four exposure regimes which characterize the reaction process. In the initial exposure regime (1), the reaction involves fluorination and etching of the 7×7 structure. In regime (2), a quasiequilibrium between etching and buildup of the reaction layer is reached. Because the substrate remains relatively crystalline in this regime, F cannot break Si-Si bonds in the substrate and there is a large amount of steric hindrance between the F atoms of neighboring SiF_2 and SiF_3 groups. Thus the reaction layer thickness is limited to ~1 ML and it is composed predominantly of SiF. As the etching reaction continues, defects form in the near-surface region of the substrate, most likely as a result of the excess heat liberated from the formation of Si-F bonds. In regime (3), the substrate becomes sufficiently disordered to disrupt the quasiequilibrium, and the reaction layer evolves to a "tree" structure of fluorosilyl chains terminated by SiF_3 groups. Steady-state etching (4) is achieved when the tree structure is completely developed. These results show that both the structure of the substrate and steric hindrance between the F atoms of neighboring SiF_x groups greatly influence the reaction process.

ACKNOWLEDGMENTS

This work was carried out in part at the National Synchrotron Light Source, Brookhaven National Laboratory, which is supported by the Department of Energy (Division of Materials Sciences and Division of Chemical Sciences, Basic Energy Sciences) under Contract No. DE-AC02-76CH0016. The authors wish to thank E. A. Carter, F. R. McFeely, F. A. Houle, H. F. Winters, and W.-C. Lin for useful discussions, and L. J. Terminello and A. Santoni for their assistance in operating the beamline. The authors also make acknowledgment to the Donors of The Petroleum Research Fund, administered by the American Chemical Society, for partial support of this research.

*Present address: Chemical Sciences Division, Lawrence Berkeley Laboratory, Berkeley, CA 94720.

[1]H. F. Winters and J. W. Coburn, Surf. Sci. Rep. **14**, 161 (1992).
[2]H. F. Winters and F. A. Houle, J. Appl. Phys. **54**, 1218 (1983).
[3]H. F. Winters and J. W. Coburn, Appl. Phys. Lett. **34**, 70 (1979).
[4]H. F. Winters and D. Haarer, Phys. Rev. B **36**, 6613 (1987).
[5]J. A. Yarmoff and F. R. McFeely, Phys. Rev. B **38**, 2057 (1988).
[6]F. R. McFeely, J. F. Morar, and F. J. Himpsel, Surf. Sci. **165**, 277 (1986).
[7]F. A. Houle, J. Appl. Phys. **60**, 3018 (1986).
[8]D. L. Flamm, D. E. Ibbotson, J. A. Mucha, and V. M. Donnelly, Solid State Technol. **4**, 117 (1983).
[9]H. F. Winters and I. C. Plumb, J. Vac. Sci. Technol. B **9**, 197 (1991).
[10]C. W. Lo, P. R. Varekamp, D. K. Shuh, T. D. Durbin, V. Chakarian, and J. A. Yarmoff, Surf. Sci. (to be published).
[11]P. C. Weakliem, C. J. Wu, and E. A. Carter, Phys. Rev. Lett. **69**, 200 (1992).
[12]J. A. Yarmoff and S. A. Joyce, Phys. Rev. B **40**, 3143 (1989).
[13]F. R. McFeely, J. F. Morar, N. D. Shinn, G. Landgren, and F. J. Himpsel, Phys. Rev. B **30**, 764 (1984).
[14]F. J. Himpsel, Y. Jugnet, D. E. Eastman, J. J. Donelon, D. Grimm, G. Landgren, A. Marx, J. F. Morar, C. Oden, R. A. Pollak, J. Schneir, and C. A. Crider, Nucl. Instrum. Methods **222**, 107 (1984).
[15]D. E. Eastman, J. J. Donelon, N. C. Hien, and F. J. Himpsel, Nucl. Instrum. Methods **172**, 327 (1980).
[16]F. J. Himpsel, F. R. McFeely, J. F. Morar, A. Taleb-Ibrahimi, and J. A. Yarmoff, in *Photoemission and Absorption Spectroscopy and Interfaces with Synchrotron Radiation,* Proceedings of the International School of Physics "Enrico Fermi," Course CVIII, Varenna, 1990, edited by M. Campagna and R. Rosei (Elsevier, Amsterdam, 1990).
[17]Ph. Avouris, F. Bozso, and A. R. Rossi, in *Photon, Beam and Plasma Stimulated Chemical Processes at Surfaces,* edited by V. M. Donnelly, I. P. Herman, and M. Hirose, MRS Symposia Proceedings No. 75 (Materials Research Society, Pittsburgh, 1987), p. 591.
[18]M. J. Bozack, M. J. Dresser, W. J. Choyke, P. A. Taylor, and J. T. Yates, Jr., Surf. Sci. **184**, L332 (1987).
[19]J. A. Yarmoff and S. A. Joyce (unpublished).
[20]C. W. Lo, D. K. Shuh, and J. A. Yarmoff (unpublished).
[21]F. J. Himpsel, P. Heimann, T.-C. Chiang, and D. E. Eastman,

Phys. Rev. Lett. **45**, 1112 (1980).
[22]D. A. Shirley, Phys. Rev. B **5**, 4709 (1972).
[23]D. V. Lang, J. D. Cohen, and J. P. Harbison, Phys. Rev. B **25**, 5285 (1982).
[24]J. Petit, M. Lannoo, and G. Allan, Solid State Commun. **60**, 861 (1986).
[25]C. J. Karlsson, E. Landemark, L. S. O. Johansson, U. O. Karlsson, and R. I. G. Uhrberg, Phys. Rev. B **41**, 1521 (1990).
[26]J. A. Yarmoff, A. Taleb-Ibrahimi, F. R. McFeely, and Ph. Avouris, Phys. Rev. Lett. **60**, 960 (1988).
[27]M. L. Knotek, Rep. Prog. Phys. **47**, 1499 (1984).
[28]H. Friedrich, B. Pittel, P. Rabe, W. H. E. Schwarz, and B. Sonntag, J. Phys. B **13**, 25 (1980).
[29]R. A. Rosenberg, J. Vac. Sci. Technol. A **4**, 1463 (1986).
[30]D. E. Ramaker, T. E. Madey, R. L. Kurtz, and H. Sambe, Phys. Rev. B **38**, 2099 (1988).
[31]J. A. Deiters and R. R. Holmes, J. Am. Chem. Soc. **112**, 7197 (1990).
[32]T. A. Schoolcraft and B. J. Garrison, J. Am. Chem. Soc. **113**, 8221 (1991).
[33]F. J. Himpsel, F. R. McFeely, A. Taleb-Ibrahimi, J. A. Yarmoff, and G. Hollinger, Phys. Rev. B **38**, 6084 (1988).
[34]F. R. McFeely, B. D. Silverman, J. A. Yarmoff, and U. O. Karlsson, in *Proceedings of the Eighth International Symposium on Plasma Chemistry, Tokyo, 1987,* edited by K. Akashi and A. Kinbara (International Union of Pure and Applied Chemistry, Tokyo, 1987).
[35]J. C. Bailar, Jr., H. J. Emeléus, R. Nyholm, and A. F. Trotman-Dickenson, *Comprehensive Inorganic Chemistry* (Pergamon, Oxford, 1973).
[36]J. R. Engstrom, M. M. Nelson, and T. Engel, Surf. Sci. **215**, 437 (1989).
[37]M. F. Hocella, Jr. and A. H. Carim, Suf. Sci. Lett. **197**, L260 (1988).
[38]H. F. Winters and J. W. Coburn, J. Vac. Sci. Technol. B **3**, 1376 (1985).
[39]V. M. Bermudez, J. Vac. Sci. Technol. A **10**, 3478 (1992).
[40]C. W. Lo, D. K. Shuh, and J. A. Yarmoff, J. Vac. Sci. Technol. A (to be published).
[41]K. Takayanagi, Y. Tanishiro, M. Takahashi, and S. Takahashi, J. Vac. Sci. Technol. A **3**, 1502 (1985).
[42]R. J. Hamers, R. M. Tromp, and J. E. Demuth, Phys. Rev. Lett. **56**, 1972 (1986).
[43]J. J. Boland and J. S. Villarrubia, Phys. Rev. B **41**, 9865 (1990).
[44]C. G. Van der Walle, F. R. McFeely, and S. T. Pantelides, Phys. Rev. Lett. **61**, 1867 (1988).
[45]T. A. Schoolcraft and B. J. Garrison, J. Vac. Sci. Technol. A **8**, 3496 (1990).
[46]C. J. Wu and E. A. Carter, Phys. Rev. B **45**, 9065 (1992).
[47]P. Guyot-Sionnest, P. Dumas, Y. J. Chabal, and G. S. Higashi, Phys. Rev. Lett. **64**, 2156 (1990).